Applied Thermal Engineering 111 (2017) 802–810

Contents lists available at ScienceDirect

Applied Thermal Engineering

journal homepage: www.elsevier.com/locate/apthermeng

Research Paper

Thermal protection method of the solar array for stratospheric airships

Junhui Meng, Zhongbing Yao, Huafei Du, Mingyun Lv *

School of Aeronautic Science and Engineering, Beihang University, 37 Xueyuan Road, Beijing 100191, PR China

HIGHLIGHTS

- Theoretical calculation, experimental test and CFD simulation are carried out for the investigation.
- The thermal protection effects of coating film, heat insulation layer and heat dissipation layer are compared.
- The output power, thermal protection effect and structure weight are comprehensively considered.

ARTICLE INFO

Article history:
Received 5 August 2016
Revised 25 September 2016
Accepted 27 September 2016
Available online 28 September 2016

Keywords:
Stratospheric airship
Multilayer thermal protection
Solar cells
Output power

ABSTRACT

Part of the sunlight energy received by the solar array on the stratospheric airship surface is converted to electric energy, and considerable energy is transformed into heat, which is bad for the envelope material and the internal pressure of the airship. It is necessary to develop different methods for the solar array to reduce its thermal effects on the stratospheric airship. Coating film, heat dissipation structure and heat insulation structure are developed to reduce the thermal effects. A series of theoretical studies are carried out to analyze the effects of three layers, especially the heat dissipation structure made up by arrayed fins, which are verified by the experimental test and CFD simulation. As for the solar array system, the mutual coordination among output power, thermal protection effect and the structure weight ought to be considered at the same time in the design of solar array system of the stratospheric airship.

1. Introduction

The stratospheric airship (SSA) is a class of Lighter-Than-Air (LTA) vehicle with application potential in communication, investigation, science exploration and other fields [1–3]. Therefore, study in the SSA has become the focus in many counties in recent years [4,5]. However, there is no mature and practical SSA in the engineering at the present stage. The energy system is one of the bottlenecks for the development of the SSA, which directly determines the long endurance flight performance of the airship [6–9]. The solar cells array, which is actually a photovoltaic (PV) array, coupling with an energy storage system is an ideal choice for the energy providing of the SSA [9].

Unfortunately, the conversion efficiency of thin film flexible solar array is around 10%, which is very low in nowadays [10]. It means that only a portion of sunlight energy received by the solar array is converted to electric energy, and considerable energy is transformed into heat, which puts the SSA a great disadvantage. The temperature difference between solar cell surface and envelop surface, where no solar array overcasts, could go up to 60 K in the daytime [11]. The heat generated by the solar array will increase the pressure of the helium inside the hull and age the envelope material underlaid the cells. In addition, the thermal performance of a stratospheric airship can have a big effect on the output performance of the solar array. Therefore, it is necessary to develop different methods for the solar array to reduce its thermal effects on the SSA.

The methods of reducing thermal effects can be divided into two types: active method and passive method. The active method is to reduce the heat generated by the thin film solar cells actively on the premise of guarantee the output electric power. And the passive one is to reduce the amount of heat transferred to the airship. As for the reducing of the heat generation, surface modification of the solar cell can be developed to restrain the penetration of the near-infrared spectrum (900–1200 nm) and increasing the transmittance of the visible light (400–800 nm) at the same time [12,13]. The methods of antireflection film and infrared cut coating preparation on the solar cells can be divided into chemical vapor deposition (CVD), physical vapor deposition (PVD), sol–gel method and so on. The transmittance of visible light for the solar cells is increased to more than 90% using different methods by a number of researchers for the past few years [14–16]. The main methods to reduce heat transferred from the solar array to the airship

* Corresponding author.
E-mail address: lv503@buaa.edu.cn (M. Lv).

http://dx.doi.org/10.1016/j.applthermaleng.2016.09.158
1359-4311/

envelope are heat insulation and heat dissipation, which have been carried out by many scholars [17–20]. The multilayer insulation (MLI) structure was carried out as early as 1950s and has been quite mature application in spacecraft [21]. Different kinds of thermal insulation coatings and materials are used on the surface of the protected objects, such as polymer sheets, reflective metal and so on [22–24]. As for the dissipation structure, plate fin heat sinks (PFHSs) are the most widely used due to their simple structure and easy manufacturing. Zhou et al. [17] investigated the thermal and hydraulic performance of 20 different plate-pin fin heat sinks with various shapes of pin cross-sections. Hung et al. [20] optimized the thermal performance of a micro-duct heat sink with a sandwich distribution porous medium using the geometric variables as search parameters. Li et al. [25] developed a thermal analysis model of composite solar array with complex structure to characterize the thermal response of the whole solar array system subjected to space heat flux. The above designs of insulation structures for other aircraft or space vehicle are referenced in this paper.

Nevertheless, the envelope of the SSA and the solar array on the surface are both flexible, which requires the thermal protection structure is also flexible. Sun et al. [10] developed a MLI material and proposed a thermal heat transfer model of flexible thin-film solar cell and MLI to study the heat insulation effects. Li et al. [26] investigated thermal insulation performance of three types of lightweight insulation substrate (LIS) subject to low ambient temperature and high solar irradiation flux conditions representative of stratospheric thermal environment for solar arrays on an airship. Li et al. [27] explored the effects of an insulation material installed between the photovoltaic array and the airship hull. They found that the insulation material may reduce the superheat of the airship hull and diurnal temperature variation of buoyancy gas, but the output of the array will decrease. The design of thermal protection structure of the solar array is not only to achieve the purpose of insulation, but also to minimize the mass of the structure. What's more, the most important premise is to guarantee the output electric power of the solar array for the SSA.

In this paper, a multilayer thermal protection (MLTP) structure including active method and passive method for solar array on the SSA is developed firstly. Theoretical models are carried out to investigate the thermal protection effects of the MLTP structure. The comparison tests and simulations using the FLUENT software of the thermal protection effects for the MLTP structure are conducted to verify the theory in the next. The thermal protection effects of coating film, heat dissipation layer and heat insulation layer are discussed respectively for contrastive analysis. A comprehensive analysis of the thermal protection structure is introduced to evaluate the overall performances of output power of the solar array, the weight of MLTP structure and its thermal protection effects.

2. The thermal protection structure of the solar array for the SSA

The MLTP structure of the solar array for the SSA studied in this paper is shown in Fig. 1, which including antireflection film, infrared cut coating, thermal insulation and dissipation layers. The antireflection film on the surface of solar array is used to increase photoelectric conversion efficiency by increasing transmittance of the visible light. The infrared cut coating is applied to reduce the transmittance of near-infrared light. In the design of the integrated film system for the solar array, SiO_2 and Ta_2O_5 are used for antireflection and cut-off, and the areal density is 5 g/m^2. The spectral response curve of the film system tested in this paper is shown in Fig. 2. It can be seen from the figure that the average transmissivity of the visible wavelengths (400–800 nm) is almost 95% and the reflectivity of near-infrared wavelengths (900–1200 nm) is close to 69%.

The heat dissipation layer of the MLTP is composed of air ducts, which are made of a series of arranged fins. The direction of the air duct is consistent with the flight direction of the SSA, so that the heat can be taken away by the airstream through the interspace between fins in the process of relative motion. As shown in Fig. 3, three kinds of fins are selected for comparison in this paper, which are long strip fin, zigzag fin and cylindrical fin. On account of the flexibility and lightweight demand for the MLTP structure, NOMEX paper honeycomb is manufactured to the fins. The heat insulation layer has the same requirement which is made of a certain thickness of paper honeycomb.

3. Thermal protection performance analysis

3.1. Theoretical analysis

The exploded view of the solar array with the MLTP structure is shown in Fig. 4, which can be divided two parts. The first part is the solar array with the optical film system. A majority of solar flux is absorbed by the solar cells, especially after coating the antireflection film. A part of the solar flux absorbed by solar cell is converted into heat energy to radiate to the external environment and transmit to the second part [26]. The second part of the structure is

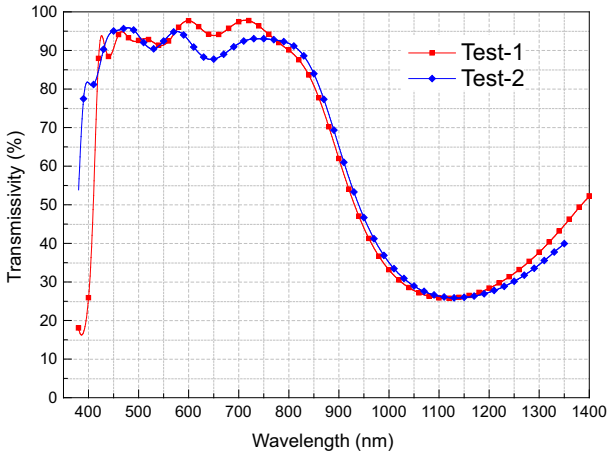

Fig. 2. Transmittance curve along with the change of wavelength.

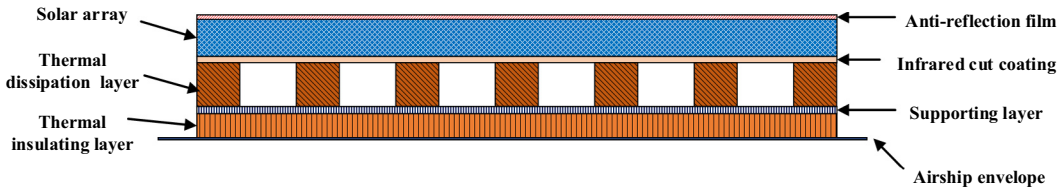

Fig. 1. The MLTP structure of the solar array for the SSA.

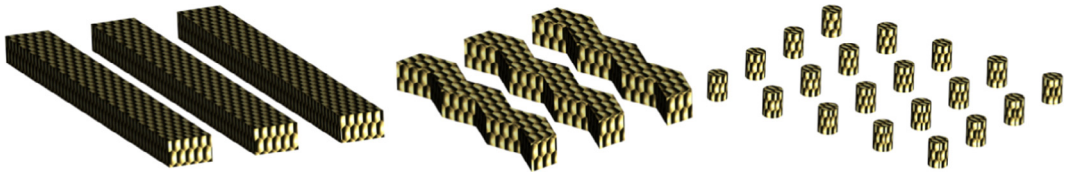

(a) The long strip fin (b) The zigzag fin (c) The cylindrical fin

Fig. 3. Three kinds of fins of the heat insulation structure.

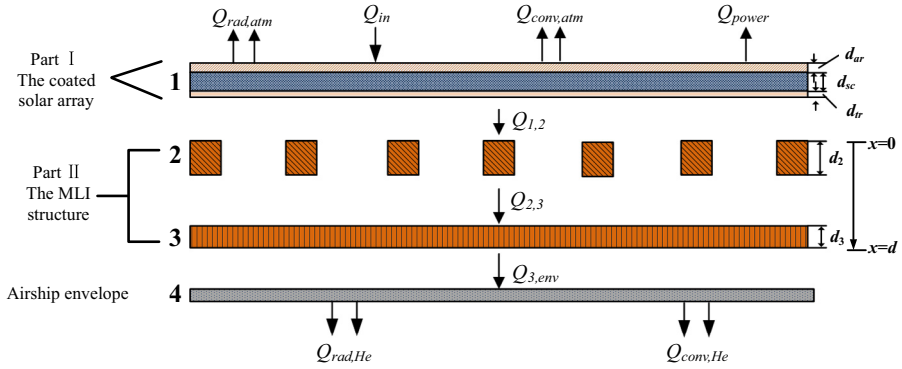

Fig. 4. The exploded view and heat transfer process of the solar array with the MLTP structure.

composed of thermal insulation and dissipation layers. After the second part, only a small part of the heat is transmitted to the airship envelope.

The heat transfer process of the system is also shown in Fig. 4. The energy equation of each layer can be received by the law of conservation of energy, which is as follows.

$$m_1 \cdot c_1 \cdot \frac{\partial T_1}{\partial \tau} = Q_{in} - Q_{rad,atm} - Q_{conv,atm} - Q_{power} - Q_{1,2} \tag{1}$$

$$m_2 c_2 \frac{\partial T_2}{\partial \tau} = Q_{1,2} - Q_{2,3} \tag{2}$$

$$m_3 c_3 \frac{\partial T_3}{\partial \tau} = Q_{2,3} - Q_{3,\mathrm{env}} \tag{3}$$

$$m_{env} c_{env} \frac{\partial T_{env}}{\partial \tau} = Q_{3,env} - Q_{rad,He} - Q_{conv,He} \tag{4}$$

where m_i is the mass of the ith layer, c_i is the specific heat of the ith layer, and T_i is the temperature the ith layer. The subscript env is the abbreviation of the airship envelope. As for each layer of the MLTP structure,

$$Q_{i,i+1} = A(T_i - T_{i+1})/(\delta_i/\lambda_i + \delta_{i+1}/\lambda_{i+1}) \tag{5}$$

$$Q_{3,env} = A(T_3 - T_{env})/(\delta_3/\lambda_3 + \delta_{env}/\lambda_{env}) \tag{6}$$

where A is the surface area of solar array, δ_i and λ_i are thickness and thermal conductivity of each layer, respectively.

If the MLTP structure of layer 2 and 3 can be taken as a whole, the Eqs. (2) and (3) can be merged into one equation,

$$m_{23} \cdot c_{23} \cdot \frac{\partial}{\partial \tau}\left(\int_0^d T'_{23}(x)dx\right) = Q_{1,2} - Q_{3,env} \tag{7}$$

The temperature gradient is considered and the temperature of this structure $T_{23}(x)$ can be calculated as follows [26,28].

$$\begin{aligned} &\lambda_{23}(T_{23}(x)) \cdot \tfrac{d^2(T_{23}(x))}{dx^2} = \tfrac{dq_x(x)}{dx} \\ &T_{23}(0) = T_1 \\ &T_{23}(d) = T_{env} \end{aligned} \tag{8}$$

where $q_x(x) = Q_{1,23}\big|_{\tau=\tau_i} - m_{23}(x) \cdot c_{23} \cdot \frac{\partial}{\partial \tau}\left(\int_0^x T'_{23}(x)dx\right)$ is the heat flux [29].

Q_{in} is the incident solar radiation energy on the solar array with coating film, including direct solar radiation, atmospheric scattering radiation, earth albedo radiation, earth infrared radiation, and so on [30,31].

The infrared radiation heat loss on the surface of thin film solar cell is given by [32]

$$Q_{rad,atm} = \varepsilon_1 \cdot A \cdot \sigma \cdot (T_1^4 - T_{air}^4) \tag{9}$$

where ε_1 is the emissivity of flexible thin-film solar cell with the antireflection coating; σ is the constant of Stefan-Boltzmann, $\sigma = 5.67 \times 10^{-8} W/(m^2 \cdot K^4)$; T_{air} is the sky equivalent temperature, K.

The convective heat loss can be described by [32]

$$Q_{conv,atm} = A \cdot h \cdot (T_1 - T_{air}) \tag{10}$$

where h is the convection heat transfer coefficient, which can be calculated as follows.

$$h = \frac{N_u \lambda_{air}}{L} \tag{11}$$

where L is the characteristic length of the solar array, m; λ_{air} is the thermal conductivity of the air,

$$\lambda_{air} = 0.0241\left(\frac{T_m}{273.15}\right)^{0.9} \tag{12}$$

$T_m = 0.5 \times (T_1 + T_s)$ is the characteristic temperature; and N_u is the Nusselt number,

$$N_u = \begin{cases} 0.54 \cdot (G_r \cdot P_r)^{1/4} & 2 \times 10^4 \leqslant G_r \cdot P_r \leqslant 8 \times 10^6 \\ 0.15 \cdot (G_r \cdot P_r)^{1/3} & 8 \times 10^6 \leqslant G_r \cdot P_r \leqslant 1 \times 10^{11} \end{cases} \tag{13}$$

where $P_r = 0.804 - 3.25 \times 10^{-4} \times T_m$ is the Prandtl number; $G_r = \left(g \cdot \alpha \cdot \Delta T_{1s} \cdot L^3\right)/\theta^2$ is the Grashof number, in which g is the acceleration of gravity, α is the coefficient of cubic expansion, and θ is the kinematic viscosity of air.

The thermal environment of the SSA is shown in Fig. 3. As shown in the figure, the energy delivered to the lifting gas through convection and infrared radiation can be described as follows, respectively [26,33,34].

$$Q_{rad,He} = A \cdot \sigma \cdot \left(\varepsilon_{\text{int}} \cdot \left(T_{env}^4 - T_{He}^4\right) + \varepsilon_{He} \cdot \left(T_{air}^4 - T_{He}^4\right)\right) \tag{14}$$

$$\varepsilon_{He} = C_{He} \cdot \varepsilon_{He}^0 \tag{15}$$

$$Q_{conv,He} = A \cdot h_{He} \cdot (T_{env} - T_{He}) \tag{16}$$

The defines of the above parameters are delivered in Ref. [26]. The output power of the solar array Q_{power} is determined by the incident solar radiation on the array and the performance characteristics of the array[35], which can be described as follows [36].

$$Q_{power} = A \cdot (I_\tau / I_0) \cdot P_0 \cdot [1 - \alpha_1 \cdot (T_1 - T_{1,0})] \tag{17}$$

where I_τ is the solar irradiance on the solar array plane at time τ, I_0 is the reference irradiance [37], P_0 is power output, per square meter, of the solar array at I_0. α_1 is the power-temperature coefficient. $T_{1,0}$ is the reference temperature of solar cell. Considering thermal effects, the conversion efficiency changes with the growing temperature [7].If the MLTP structure can be seen a whole, $Q_{1,2}$ and $Q_{3,env}$ can be received from Eqs. (5) and (6). The equivalent thermal conductivity of the MLTP structure can be given

$$\lambda_{MLTP} = \frac{(d_2 + d_3)}{(\theta_{HC} + \theta_{air}) \cdot A} \tag{18}$$

where θ_{HC} and θ_{air} are the thermal resistance of honeycomb and air for the MLTP structure, respectively.

The theoretical calculation is carried out using Matlab based on the given material parameters. The temperatures of each layer can be received by solving Eqs. (1), (7) and (4). The temperature difference between solar array and envelope material is the research emphasis.

3.2. Experimental approach

An experimental test is carried out to verify the thermal protection effect of the MLTP, as well as to calculate the thermal conductivity of flexible thin-film solar cell and Nomex honeycomb accurately [10,26]. The test sample studied in this paper is composed of solar cells, MLTP structure and the envelope material, which is shown in Fig. 5. Among them, solar cells with and without coating film are tested respectively, and the MLTP structure includes heat dissipation structure and heat insulation structure. Six thermocouples are used to detect temperature of the upper and lower surfaces of the solar array system.

The dimensions of environmental cabin are $D \times L = 1.8\ \text{m} \times 3.5\ \text{m}$. Two pieces of test samples can be put in the environmental cabin at a time, and their dimensions are $0.24\ \text{m} \times 0.22\ \text{m}$. The environmental temperature is set as 216 K and the pressure is 3 KPa in the environmental cabin in the whole test process. The solar radiation simulated by the solar simulator irradiates on upper surface of the samples in the flux range of 300–1260 W/m^2 [26]. And solar radiation of 891 W/m^2 and 1260 W/m^2 are the research emphasis, which are the average and maximum value in the stratosphere. Temperature data are recorded by temperature inspection instrument every five minutes until temperature change <1 °C/10 min.

3.3. Simulation analysis

The simulation using the FLUENT software is carried out to study the thermal protection effects of the MLTP structure and compare the heat dissipation effects of three different air ducts.

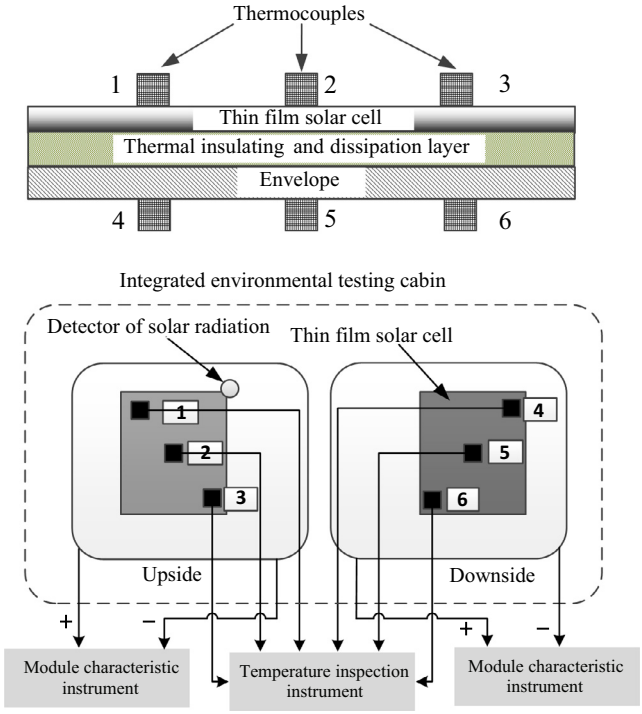

Fig. 5. The schematic diagram of the test.

The standard turbulence model is used in the simulation. The basic governing equations are employed are shown as follows.

The continuity equation is

$$\frac{\partial}{\partial x_i}(\rho u_i) = 0 \tag{19}$$

The momentum equation is

$$\frac{\partial(\rho u_i u_j)}{\partial x_j} = -\frac{\partial p}{\partial x_i} + \frac{\partial}{\partial x_j}\left(\mu \frac{\partial u_i}{\partial x_j} - \rho u_i u_j\right) \tag{20}$$

The energy equation is

$$\frac{\partial(\rho u_i u_j)}{\partial x_j} = -\frac{\partial p}{\partial x_i} + \frac{\partial p}{\partial x_j}\left(\mu \frac{\partial u_i}{\partial x_j} - \rho u_i u_j\right) \tag{21}$$

The turbulent kinetic energy (TKE) equation is

$$\rho \frac{dk}{dt} = \frac{\partial}{\partial x_i}\left[\alpha_k \mu \frac{\partial k}{\partial x_i}\right] + G_k + G_b - \rho\varepsilon - Y_M \tag{22}$$

The model with non-uniformity grids is carried out to increase the computational efficiency and improve the accuracy. Because speed and temperature in the air duct change sharply, the mesh in this block is quite tense. The entrance is set as velocity boundary condition and the type, velocity and temperature of the inlet fluid should be set. The governing equations are discretized by control volume integration method. The influence of turbulence on performance of flow and heat transfer is considered in k-ε two-equation model. Implicit solution by variable separation method is developed to ensure the stability of convergence. The coupling equations of pressure and velocities were solved with the SIMPLE algorithm.

The parameters of airflow is set according to the stratospheric environment. The temperature is 217 K, density is 0.088 kg/m^3, viscosity is 1.42×10^{-5} kg/m s, thermal conductivity is 2.035×10^{-5} W/m K, specific heat capacity is 1.013×10^3 J/kg K, and the material of the fin is NOMEX paper honeycomb.

4. Results and discussion

4.1. Comparison of theory, experiment and simulation

The theoretical results of the envelope material temperature with and without the thermal protection structure are shown in Fig. 6. As shown in the figure, the maximum temperature of the envelope without protection can reach 338.12 K, which is much higher than ones with thermal protection. And that is to say the thermal protection structure can decrease the envelope material temperature distinctly, which can relieve the superthermal and overpressure problems of the airship. In addition, the temperature with mixed protection structure ($d_2 = 3$, $d_3 = 5$) is the lowest, which is $T_{env} = 287.10$ K. And the thermal protection effect of the heat insulation layer ($d_2 = 0$, $d_3 = 8$, $T_{env} = 295.36$ K) is better than the heat dissipation layer ($d_2 = 8$, $d_3 = 0$, $T_{env} = 301.13$ K).

In order to verify the accuracy of the theory and simulation, the comparison among the results of the theory, experiment and simulation is carried out for the MLTP structure. The relationship of the temperature difference and the solar radiation flux is shown in Fig. 7. As shown in the figure, the results from theoretical calculation and the simulation have good agreement with experiment, in spite that the simulation results are slightly bigger with deviations of about 6%. In particular, there is low accuracy in the low solar radiation for the experimental results. The possible reason

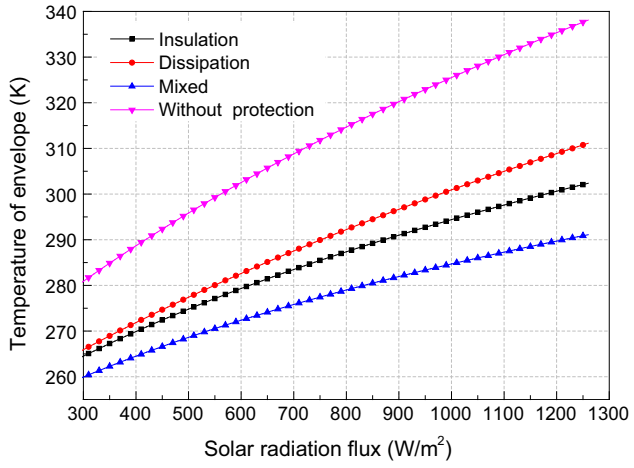

Fig. 6. Temperature of envelope with and without the thermal protection structure.

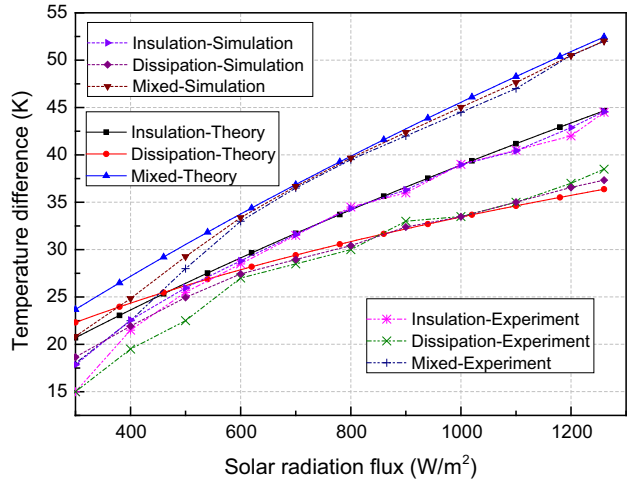

Fig. 7. Relationship of the temperature difference and the solar radiation flux.

is that infrared radiation of the earth and clouds is considered in the theoretical model, while the environmental chamber in the test just can simulate solar radiation. The fitness of the model increases with the increase of solar radiation flux, because the infrared radiation is a small amount relative to the solar radiation.

The simulation result of the temperature distribution for the MLTP structure in solar radiation flux of 1260 W/m^2 is shown in Fig. 8. As shown in Fig. 6, the initial temperature of the envelope material is set as 338.12 K, which can be reduced to 286 K, and similar with 287.10 K received by the theoretical calculation.

4.2. Thermal protection performance analysis

4.2.1. The coating film performance

The surface treatment of solar array is coating visible antireflective film and infrared cut-off film. The antireflective film is used to increase the visible transmittance (VT) by reducing its reflection and the infrared cut-off film is used to increase the infrared reflectivity (IR) to reduce the generation of heat. Figs. 9 and 10 shows the effects of IR and VT on the temperature difference and output power. As shown in Fig. 9, the temperature difference and output power increase gradually with the increase of IR from 0.2 to 0.95. Furthermore, the influence of IR on the output power is not significant in the low solar radiation flux. Similarly, the temperature difference and output power also increase with the increase of VT from 0.8 to 0.95. It is the thermal effect that affect the output power for the change of IR, but the photoelectric conversion efficiency for the change of VT.

4.2.2. Heat dissipation effects

To compare three kinds of air ducts, heat transfer amount, heat transfer coefficient, Nusselt number, TKE and pressure drop are chosen for the comparison in different air speeds. The analysis results are shown in Tables 1–3. As shown in the tables, five parameters studied increase with the increase of the air speed for the same air duct. The results of different ducts show that the heat transfer amount of long strip duct is maximum and the cylindrical duct is minimum. The possible reason is that the heat transfer amount is related to the air flow through duct in per unit time, and the cylindrical duct is array structure, which is bad for stream guidance. The cylindrical duct owns the maximum values for three parameters i.e. heat transfer coefficient, Nusselt number and the TKE, and the zigzag duct is the minimum one. As for the pressure drop, the long strip duct is almost as same as the zigzag duct, which is larger than the cylindrical duct. Although the wall of cylindrical duct is incontinuous, the secondary divided flow makes three parameters increase.

To further illustrate the comprehensive performance of the air ducts, heat transfer factor j and friction factor f are introduced, which are shown as follows.

$$j = \frac{Nu}{RePr^{1/3}} \tag{23}$$

$$f = \frac{2\Delta pD}{l\rho v^2} \tag{24}$$

where D is width of the duct, l is length of the duct, ρ and v are density and speed of the fluid, respectively.

It can be seen from Fig. 11 that the heat transfer factor and friction factor both decrease with the increase of air speed. The heat transfer factors of cylindrical air duct in different temperatures are greatest and the long strip air duct takes second place. While as for the friction factor, the relationship of three kinds of ducts is opposite. Comprehensive analysis of the heat transfer factor and friction factor, the cylindrical air duct has a better performance. The simulation results for three ducts are shown in

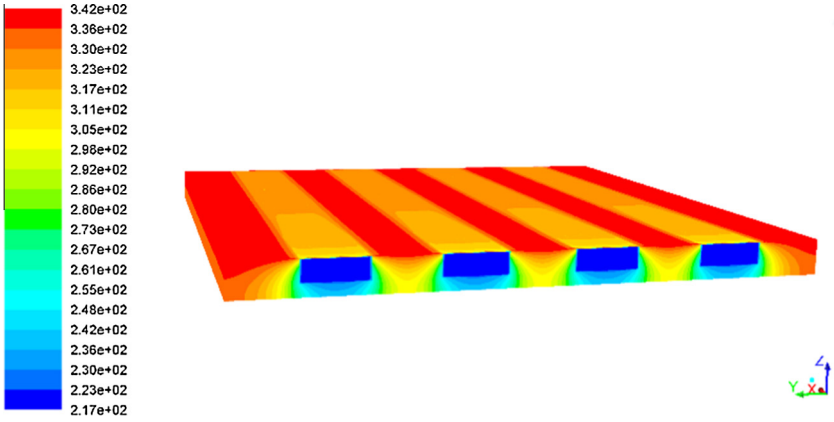

Fig. 8. Temperature distribution of the MLTP structure.

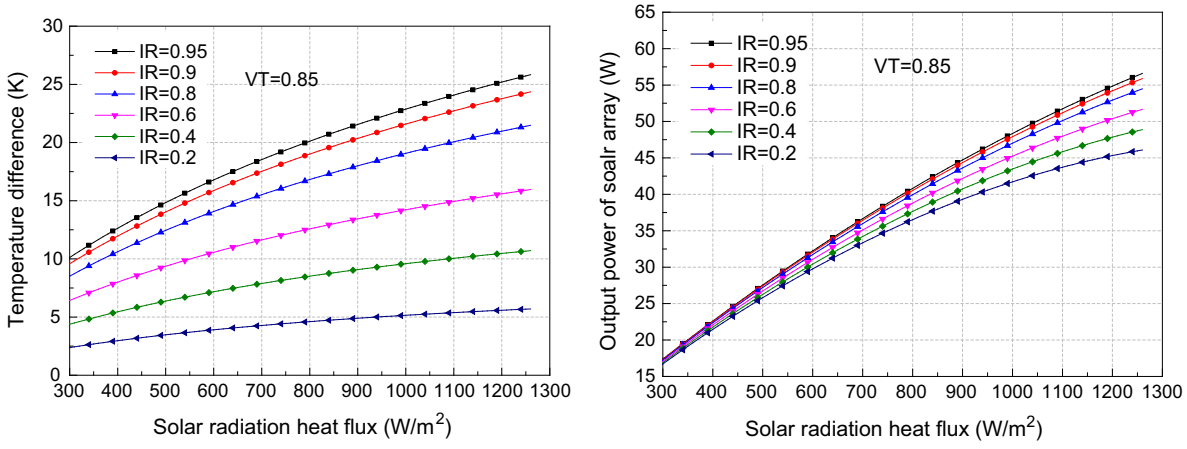

Fig. 9. Effects of IR on the temperature difference and output power.

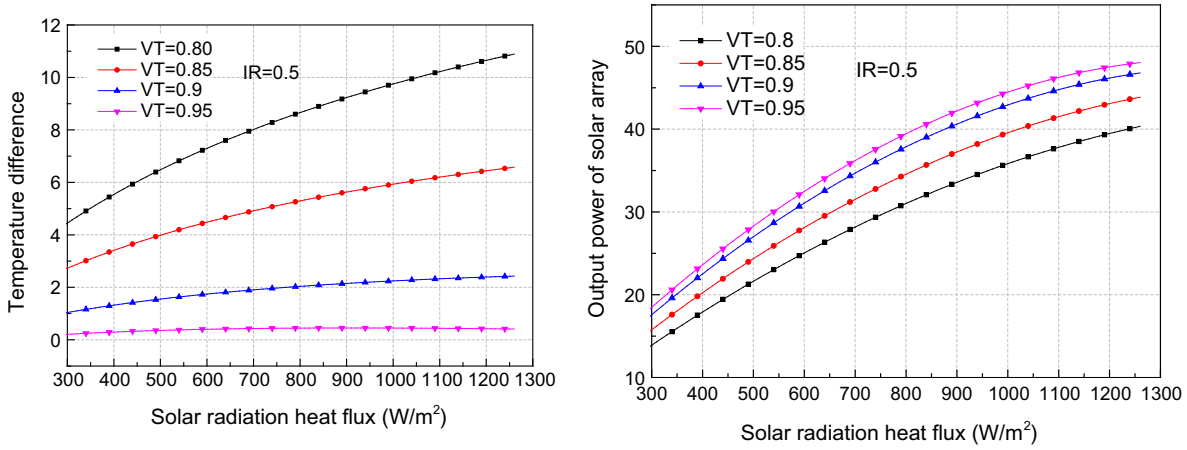

Fig. 10. Effects of VT on the temperature difference and output power.

Table 1
The heat insulation performance of the long strip air duct in different air speeds.

Air speed (m/s)	Heat transfer amount (W)	Heat transfer coefficient (W/m^2-k)	Nusselt number Nu	TKE K (m^2/s^2)	Pressure drop △P (Pa)
5	79.47	2.27	134.06	0.17	319.37
10	87.57	3.13	194.79	0.57	322.54
15	93.89	4.041	259.41	1.149	327.25
20	98.19	4.88	320.25	1.918	333.39

Table 2
The heat insulation performance of the zigzag air duct in different air speeds.

Air speed (m/s)	Heat transfer amount (W)	Heat transfer coefficient (W/m^2-k)	Nusselt number Nu	TKE K(m^2/s^2)	Pressure drop △P (Pa)
5	67.57	1.77	107.41	0.11	319.32
10	73.11	2.34	147.38	0.34	322.50
15	76.99	2.96	192.14	0.68	327.25
20	79.56	3.54	234.46	1.11	333.44

Table 3
The heat insulation performance of the cylindrical air duct in different air speeds.

Air speed (m/s)	Heat transfer amount (W)	Heat transfer coefficient (W/m^2-k)	Nusselt number Nu	TKE K(m^2/s^2)	Pressure drop △P (Pa)
5	9.02	3.71	245.78	0.33	0.51
10	9.42	5.25	358.82	1.30	3.34
15	9.88	6.89	479.09	2.84	6.83
20	10.22	8.45	593.93	4.94	11.44

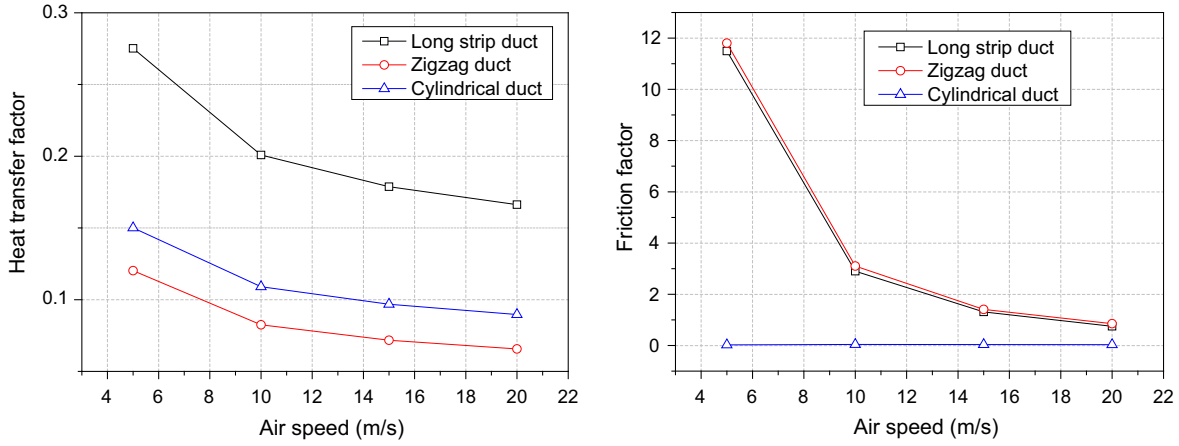

Fig. 11. (a) Heat transfer factor and (b) friction factor in different air speeds.

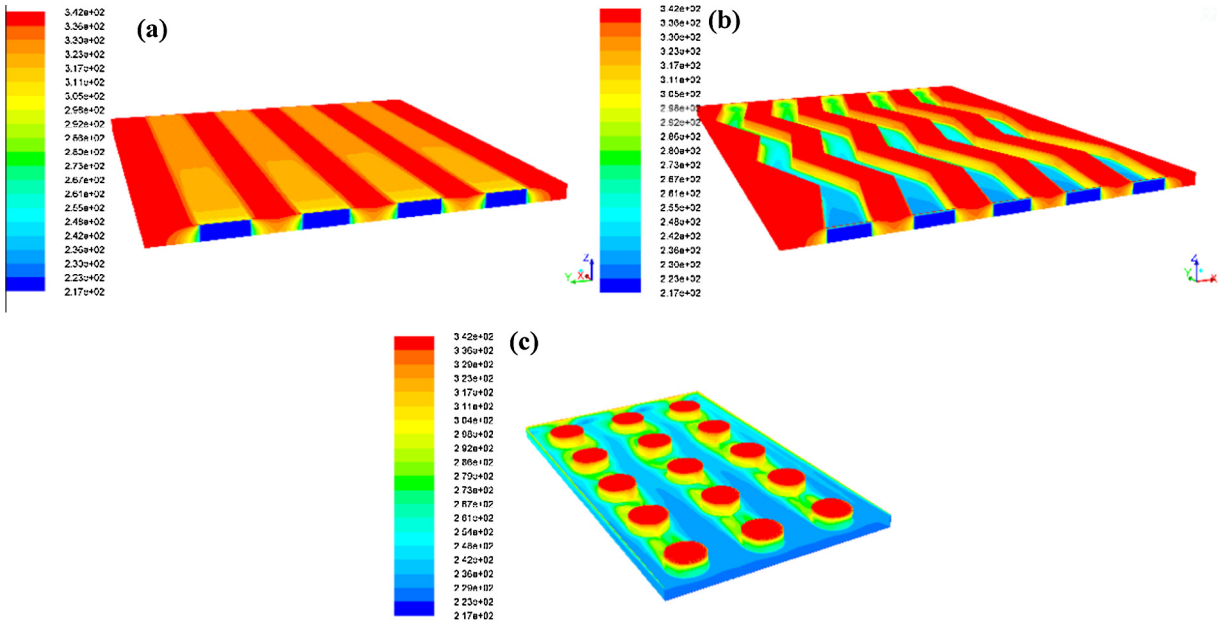

Fig. 12. The temperature distributions of (a) long strip duct, (b) zigzag duct and (c) cylindrical duct.

Fig. 12. As shown in the figure, the secondary divided flow is obvious and the temperature in bottom of the MLTP is the lowest one. However, the noncontinuity of the cylindrical duct makes it difficult to manufacture, because fins of the air ducts are made of paper honeycomb, which increases the production cost greatly. The long strip air duct is used for future analysis in this paper.

4.2.3. Heat insulation effects

Fig. 13 shows the thermal protection effect of the insulation structure with different thickness. As shown in the figure, the thermal protection effect of 3 mm insulation structure is not very ideal and the variation curve is relatively flat, which means the temperature difference has little change with the variation of solar radiation. When the thickness of insulation structure reaches to 8 mm, the thermal protection effect is relatively obvious.

4.2.4. Comprehensive performance of the thermal protection structure

The solar cells produce a lot of heat in the process of photoelectric conversion, which is bad for solar cells themselves and the envelope material of the SSA. Because the thermal protection performance and lightweight are both requirement for the MLTP structure, a specific temperature difference is defined to indicate the temperature reduced by the MLTP structure and its areal density.

$$\xi = \frac{T_1 - T_{env}}{\rho_{MLTP}} \tag{25}$$

The comparison of specific temperature difference among different thermal protection methods is shown in Table 4. As shown in the table, although the temperature difference of insulation layer is bigger than the dissipation layer, its areal density is bigger too. So the specific temperature difference of the insulation layer is almost equal to the dissipation layer. Coating film on the surface of the solar array is a method to improve absorptivity of the visible light and reflectivity of infrared light. As a result, the photoelectric conversion efficiency of solar cells increase, and their temperature decrease at the same time. Although the heat insulation effect of coating film is little, on the premise of making comprehensive consideration for output power, the heat protection effect and the structure weight, it is still an available method, because the specific temperature difference of the coating film is significant.

It is necessary to take the output power of the solar array into account to consider the comprehensive performance of the MLTP structure. Several parameters concerned in this paper are presented in Fig. 14, including the temperature of solar array, specific temperature difference, output power with and without considering temperature effect.

As shown in the figure, the temperatures of solar array vary nonlinearly with solar radiation flux irradiating on the sample, with gradually slow increasing rate. However, tendency of the specific temperature difference with solar radiation flux is

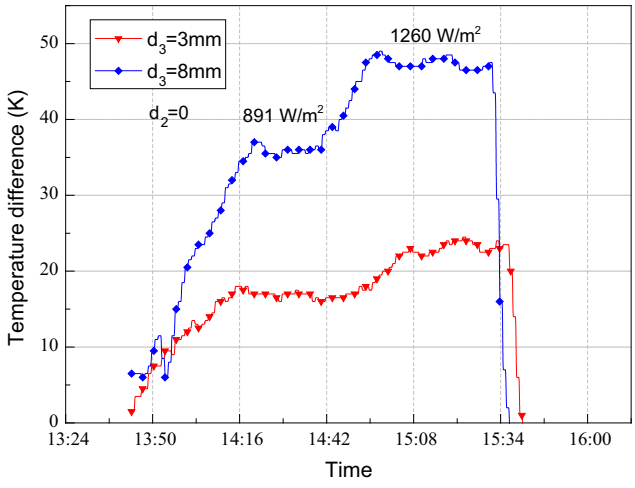

Fig. 13. Thermal protection effect of the insulation structure with different thickness.

Table 4
Comparison of different thermal protection methods.

Thermal protection method	Areal density (g/m^2)	Temperature difference (K)		Specific temperature difference (K/(g/m^2))	
		891	1260	891	1260
Coating film	5	11.32	15.56	2.26	3.11
Insulation layer	346	35.90	43.07	0.10	0.14
Dissipation layer	263	27.65	33.82	0.11	0.13

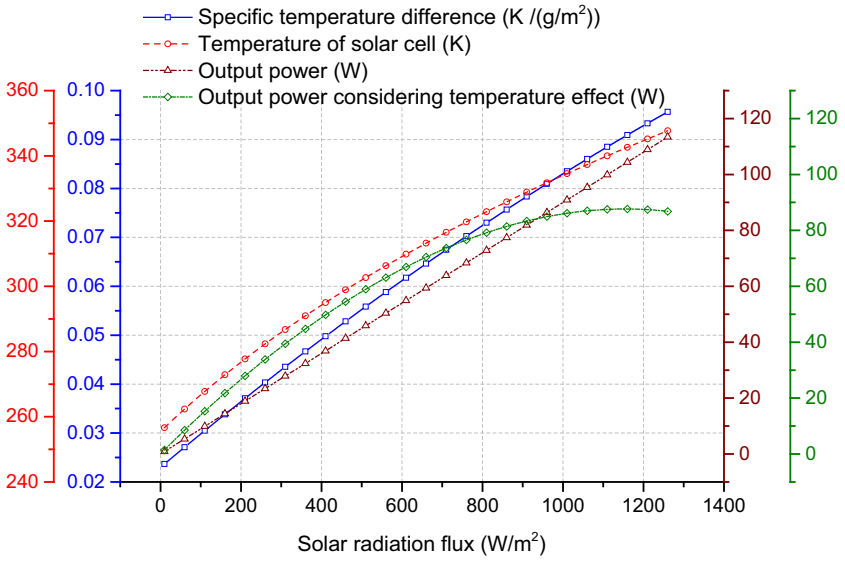

Fig. 14. Comprehensive performance of the solar array system.

approximately linear. It is found that significant difference exits between two kinds of output power with and without considering the temperature effect. Compared with output power without considering the temperature effect, the output power increases rapidly and decreases gradually with increasing of solar radiation flux when the temperature effect is considered. It can be inferred that the output power is still unable to growth even if the solar radiation flux increases after a certain level of growth, which suggests that the need for further optimization of the MLPT structure.

5. Conclusions

(1) In order to explore the thermal protection effects of the MLTP structure, theoretical study, experimental investigation and simulation analysis are carried out in this paper. By contrasting theoretical calculation and test data, calculating method is validated for the use of equivalent conductivity. The coating film, heating dissipation and insulation layers are investigated, respectively. In addition, the specific temperature difference is defined as the ratio of the temperature difference between the top and bottom of the MLTP structure and the areal density of the solar array system with the MLTP structure.

(2) It is found that the IR affects the output power by altering the thermal absorption of solar array, but by altering the photoelectric conversion efficiency for the VT. The cylindrical duct has good heat dissipation performance because of the secondary divided flow. But the poor manufacturability and high cost of the uncontinuous paper honeycomb limit its practical application. The thermal protection effect of the insulation layer increases with the increasing of its thickness, which is better than the heat dissipation layer.

(3) The mutual coordination among output power, heat insulation effect and the structure weight ought to be considered at the same time in the design of solar array system of the SSA. To a certain extent, the coating film can improve the output power, but it is not obvious to reduce the heat absorption. Because the weight increasing caused by the coating film almost can be ignored, it is an alternative method. Multi-layer structure composed by heat insulation layer and heat dissipation layer can effectively reduce the heat transmission to envelope material from solar array. The structure and geometry size should be optimized to receive the best specific temperature difference in the future.

Acknowledgements

This work was supported by the National Natural Science Foundation of China under Grant No. 51307004. The authors thank all the people involved in the past and present progress of the experiment. The authors also are grateful to the reviewer and the executive editor for their precious suggestions about this paper.

References

[1] S.D. Ilcev, Stratospheric communication platforms as an alternative for space program, Aircraft Eng. Aerospace Technol. 83 (2011) 105–111.
[2] M.S. Smith, E.L. Rainwater, Applications of scientific ballooning technology to high altitude airships, in: Proceedings 3rd Annual Technical Forum, American Institute of Aeronautics and Astronautics, 2003 (November).
[3] L. Jamison, G.S. Sommer, I.R. Porche III, High-altitude airships for the future force army, in: DTIC Document, 2005.
[4] C. Stockbridge, A. Ceruti, P. Marzocca, Airship research and development in the areas of design, structures, dynamics and energy systems, Int. J. Aeronaut. Space Sci. 13 (2012) 170–187.
[5] Y.-G. Lee, D.-M. Kim, C.-H. Yeom, Development of Korean high altitude platform systems, Int. J. Wireless Inf. Networks 13 (2006) 31–42.
[6] K. Sun, M. Zhu, Q. Liu, Membrane material-based rigid solar array design and thermal simulation for stratospheric airships, Adv. Mater. Sci. Eng. 2014 (2014) 1–7.
[7] J. Li, M. Lv, D. Tan, W. Zhu, K. Sun, Y. Zhang, Output performance analyses of solar array on stratospheric airship with thermal effect, Appl. Therm. Eng. 104 (2016) 743–750.
[8] Y. Wang, C. Yang, A comprehensive numerical model examining the thermal performance of airships, Adv. Space Res. 48 (2011) 1515–1522.
[9] A. Colozza, J. Dolce, Initial Feasibility Assessment of a High Altitude Long Endurance Airship, 2003.
[10] K. Sun, Q. Yang, Y. Yang, S. Wang, J. Xu, Q. Liu, Y. Xie, P. Lou, Thermal characteristics of multilayer insulation materials for flexible thin-film solar cell array of stratospheric airship, Adv. Mater. Sci. Eng. 2014 (2014) 1–8.
[11] X. Xinlin, L. Defu, Y. Xiaochuan, Thermal characteristics of stratospheric aerostats and their research, Acta Aeronaut. Astronaut. Sin. 4 (2009) 002.
[12] C. Ballif, J. Dicker, D. Borchert, T. Hofmann, Solar glass with industrial porous SiO_2 antireflection coating: measurements of photovoltaic module properties improvement and modelling of yearly energy yield gain, Sol. Energy Mater. Sol. Cells 82 (2004) 331–344.
[13] T.K. Boström, E. Wäckelgård, G. Westin, Anti-reflection coatings for solution-chemically derived nickel—alumina solar absorbers, Sol. Energy Mater. Sol. Cells 84 (2004) 183–191.
[14] M.J. Ariza, F. Martin, D. Leinen, XPS surface analysis of monocrystalline silicon solar cells for manufacturing control, Appl. Phys. Mater. Sci. Proc. 73 (2001) 579–584.
[15] Z. Zhang, Y.Y. Wang, J. Zhu, X.M. Wu, R.Y. Zhang, Broadband and omnidirectional antireflection of SiN composite nanostructures-decorated Si surface for highly efficient Si solar cells, J. Nanophotonics 9 (2015) 8.
[16] A.J. Haider, A.A. Najim, M.A.H. Muhi, TiO2/Ni composite as antireflection coating for solar cell application, Opt. Commun. 370 (2016) 263–266.
[17] F. Zhou, I. Catton, Numerical evaluation of flow and heat transfer in plate-pin fin heat sinks with various pin cross-sections, Numer. Heat Transf. Part A Appl. 60 (2011) 107–128.
[18] P.V.S.S. Srivatsa, R. Baby, C. Balaji, Numerical investigation of PCM based heat sinks with embedded metal foam/crossed plate fins, Numer. Heat Transf. Part A: Appl. 66 (2014) 1131–1153.
[19] D.A. McNeil, A.H. Raeisi, P.A. Kew, R.S. Hamed, An investigation into flow boiling heat transfer and pressure drop in a pin–finned heat sink, Int. J. Multiph. Flow 67 (2014) 65–84.
[20] T.-C. Hung, W.-M. Yan, Optimization of design parameters for a sandwich-distribution porous-microchannel heat sink, Numer. Heat Transf. Part A Appl. 66 (2014) 229–251.
[21] H.K. Kim, C.Y. Han, Analytical and numerical approaches of a solar array thermal analysis in a low-earth orbit satellite, Adv. Space Res. 46 (2010) 1427–1439.
[22] Z. Liu, Y.Z. Li, F.S. Xie, K. Zhou, Thermal performance of foam/MLI for cryogenic liquid hydrogen tank during the ascent and on orbit period, Appl. Therm. Eng. 98 (2016) 430–439.
[23] R.C. Youngquist, M.A. Nurge, W.L. Johnson, S.O. Starr, Modeling transmission effects on multilayer insulation, J. Therm. Sci. Eng. Appl. 7 (2015) 7.
[24] G. Salvalai, M. Imperadori, D. Scaccabarozzi, C. Pusceddu, Thermal performance measurement and application of a multilayer insulator for emergency architecture, Appl. Therm. Eng. 82 (2015) 110–119.
[25] J. Li, S. Yan, R. Cai, Thermal analysis of composite solar array subjected to space heat flux, Aerosp. Sci. Technol. 27 (2013) 84–94.
[26] J. Li, M. Lv, K. Sun, W. Zhu, Thermal insulation performance of lightweight substrate for solar array on stratospheric airships, Appl. Therm. Eng. 107 (2016) 1158–1165.
[27] X. Li, X. Fang, Q. Dai, Research on thermal characteristics of photovoltaic array of stratospheric airship, J. Aircraft 48 (2011) 1380–1386.
[28] G.A. Greene, Y.I. Cho, J.P. Hartnett, A. Bar-Cohen, Advances in Heat Transfer, Academic Press, 2006.
[29] C.-H. Yan, S.-H. Meng, G.-Q. Chen, W. Qu, G.-Q. Liu, Steady heat transfer analysis of multilayer thermal insulations for metallic thermal protection system, J. Aerosp. Power 5 (2006) 002.
[30] F. Kreith, J.F. Kreider, Numerical Prediction of the Performance of High Altitude Balloons, Atmospheric Technology Division, National Center for Atmospheric Research, 1974.
[31] R.E. Farley, BalloonAscent: 3-D simulation tool for the ascent and float of high-altitude balloons, AIAA 7412 (2005) 2005.
[32] Q. Dai, X. Fang, X. Li, L. Tian, Performance simulation of high altitude scientific balloons, Adv. Space Res. 49 (2012) 1045–1052.
[33] W. Yao, X. Lu, C. Wang, R. Ma, A heat transient model for the thermal behavior prediction of stratospheric airships, Appl. Therm. Eng. 70 (2014) 380–387.
[34] L.A. Carlson, W.J. Horn, New thermal and trajectory model for high-altitude balloons, J. Aircraft 20 (1983) 500–507.
[35] Z. Lixue, W. Zhongwei, Y. Xixiang, Selecting stratospheric airship energy storage system using analytic hierarchy process and physical programming, Proc. Inst. Mech. Eng. Part G: J. Aerosp. Eng. 228 (2014) 2508–2515.
[36] S. Chen, B. Song, H. Wang, Exploring optimum power unit of propulsion system for high altitude airship, Proc. Inst. Mech. Eng. Part G: J. Aerosp. Eng. 229 (2014) 301–311.
[37] E. Matz, J. Appelbaum, Y. Taitel, D.J. Flood, Solar cell temperature on Mars, J. Propul. Power. 14 (1998) 119–125 (0748–4658).